CHEMISTRY OF MATERIALS
Article

Chem. Mater. **2010,** *22,* 5687–5694 5687
DOI:10.1021/cm101502n

Bottom-up Approach toward Titanosilicate Mesoporous Pillared Planar Nanochannels for Nanofluidic Applications

Marco Faustini,[†] Marylene Vayer,[‡] Benedetta Marmiroli,[§] Marc Hillmyer,[∥] Heinz Amenitsch,[§] Christophe Sinturel,[‡] and David Grosso*,[†]

[†]*Laboratoire Chimie de la Matière Condensée de Paris, UMR UPMC−CNRS 7574, Université Pierre et Marie Curie (Paris 6), Collège de France, 11 place Marcelin Berthelot, 75231, Paris, France,* [‡]*Centre de Recherche sur la Matière Divisée, 1b rue de la Férollerie, 45 071 Orléans Cedex 02, France,* [§]*Institute of Biophysics and Nanosystem Research, Austrian Academy of Sciences, Schmiedlstrasse 6, 8042 Graz, Austria, and* [∥]*Department of Chemistry, University of Minnesota, 207 Pleasant Street SE, Minneapolis, Minnesota 55455-0431*

Received May 29, 2010. Revised Manuscript Received July 26, 2010

Nanofluidic transport in lab-on-chip devices requires nanochannels that are difficult to fabricate since they require challenging top-down technological approaches. We present a bottom-up, scalable, low-cost, and robust alternative to construct large areas of extremely homogeneous Pillared Planar Nanochannels (PPNs) for nanofluidic applications. Their unique structure is made of mesoporous titanosilicate pillars, of 20 nm in diameter, supporting a continuous sealing layer of the same material. This complex hierarchical structure is achievable when combining diverse bottom-up processing strategies that include self-assembly of block copolymer, nanostructured sol−gel coatings, and highly controlled liquid deposition processing, with powerful top-down techniques such as deep X-ray lithography. While these novel materials are of interest for many nanotechnological applications, we focus on their ability to guide fluids through natural capillary forces, for which the classical Washburn's model of diffusion is verified. These systems are the first promising example of fully mesoporous materials applied to nanofluidics, thus opening the "lab-on-chip" domain to *mesofluidics*.

1. Introduction

The development of novel integrated nanomaterials is driven by economical, ecological, and social pressures to handle miniaturized high technology devices, especially in domains requiring ultrafast technological evolution, such as microelectronics, medical therapy or diagnosis, and energy conversion. These nanomaterials will also play a key role in the future of emerging technologies such as micro and nanofluidics.[1] As a consequence, material chemists are challenged to synthesize and integrate smaller and smaller pieces of matter into more and more complex architectures and at the lowest possible cost. To achieve this goal, "top-down" and "bottom-up" approaches exist with advantages and drawbacks related to cost-effectiveness, scalability, lateral and transverse resolutions, long-range order, and compatibility, making them often complementary.[2] Systems for which surfaces with complex structures and topographies at micro- and nanoscales are required are lab-on-chip devices, also termed micro- and nanofluidics systems. In analogy with microprocessors in microelectronics, several miniaturized basic units are needed (e.g., pumps, gates, and containers) to construct a fully functional device.[3] Fluid transport is generally implemented in the form of sealed ducts such as planar nanochannels that are exclusively manufactured by "top-down" methods. The kinetics of fluid and solute diffusion within these channels are mainly governed by the channel's dimension, morphology, and surface chemistry. These properties would be further modulated if nanopillars, and their additional functionalized interfaces, could be intercalated between the top and bottom surfaces of the channels. Indeed, it is well established that very dense pillar arrays scaled down to submicrometer sizes are a prerequisite for high performance fluidic devices.[4] While manufacturing these complex multiscale nanostructures by top-down technologies is extremely challenging, time-consuming, and often restricted to small areas, part of the fabrication process could be replaced by straightforward bottom-up approaches. Indeed, natural molecular self-assembly is a very simple and versatile method to obtain large areas of ordered, functionalized nanomotifs such as nanopores,[8] nanocraters,[5] or even nanopillars.

*To whom correspondence should be addressed. E-mail: david.grosso@upmc.fr. Phone: 33 (0) 1 44 27 15 30. Fax: 33 (0) 1 44 27 15 04 (14 43).

(1) Van den Berg, A.; Craighead, H. G.; Yang, P. *Chem. Soc. Rev.* **2010**, *39*, 899–900.
(2) Innocenzi, P.; Kidchob, T.; Falcaro, P.; Takahashi, M. *Chem. Mater.* **2008**, *20*, 607–614.
(3) Mark, D.; Haeberle, S.; Roth, G.; von Stettenzab, F.; Zengerlez, R. *Chem. Soc. Rev.* **2010**, *39*, 1153–1182.
(4) Lavrik, N. V.; Taylorb, L. C.; Sepaniak, M. J. *Lab Chip* **2010**, *10*, 1086–1094.
(5) Kuemmel, M.; Allouche, J.; Nicole, L.; Boissière, C.; Laberty, C.; Amenitsch, H.; Sanchez, C.; Grosso, D. *Chem. Mater.* **2007**, *19*, 3717–3725.

Published on Web 09/27/2010

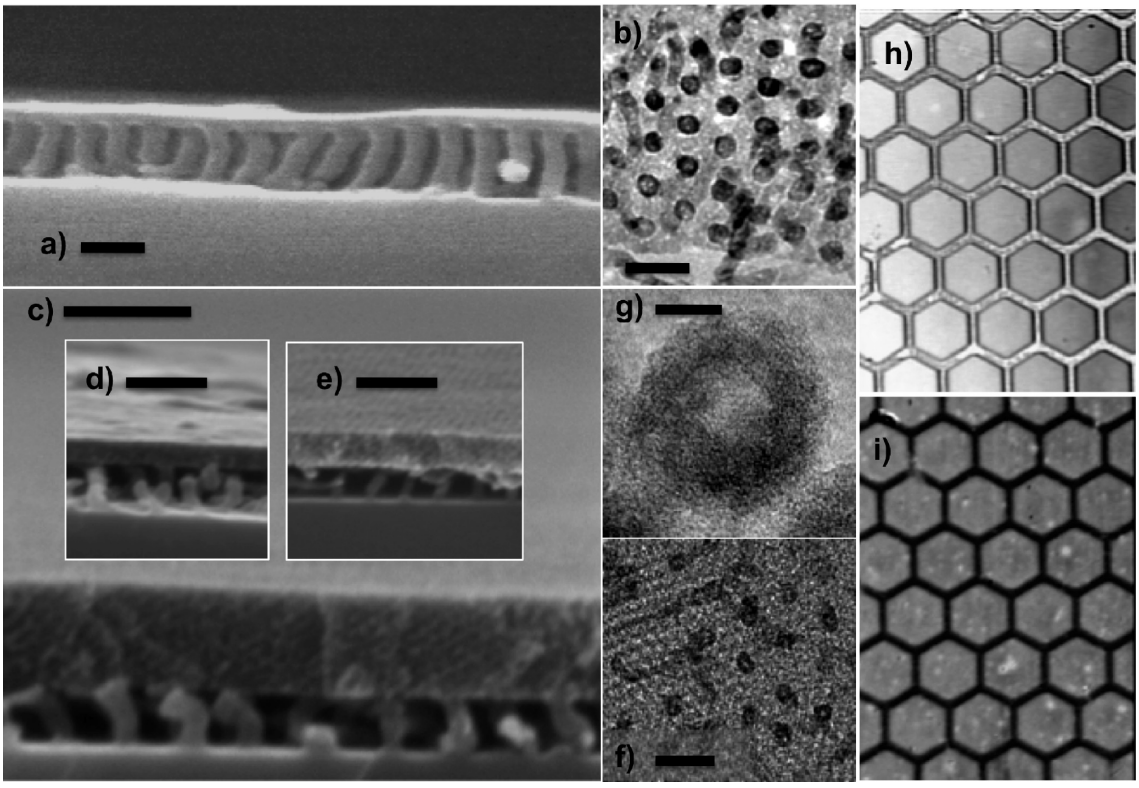

Figure 1. Electronic and optical microscopy images of typical PPNs layers with various chemical compositions, inner structure and morphologies. (a, b) SEM (profile cut) and TEM (top view) images respectively of a pure TiO_2 PPN. Images (c−f) were taken from (F127-templated) 10%SiO_2-90%TiO_2 systems. SEM images (c−e) display profile cuts, showing roofs of different thicknesses, but all bearing the same ordered mesoporosity with *Im3m* space group. TEM images (f, g) are top views of the layer, revealing a clear hollow structure of the pillars. Scale bars = 50 nm for (a, b, f); 100 nm for (c, d, e); and 5 nm for (g). (h, i) Optical images of pure PS porous membrane and PPN, respectively, after X-ray lithography and leaching. The continuous part corresponds to the irradiated zones where materials have been stabilized. The hexagonal motifs have a dimension of 40 μm.

Here we construct large areas of *mesofluidic* Pillared Planar Nanochannels (PPNs), which are made of vertical nanopillars with controlled dimensions, porosity, and chemical composition supporting a continuous sealing layer of the same material. Electronic microscope images displayed in Figure 1panels a−g illustrate the latter morphology for dense TiO_2 (panels a,b) and mesoporous titanosilicate (panels c−g) systems. Nanopillars, separated by around 40 nm and supporting a roof layer of the same material, are clearly observed on the profile cuts (panels a, c, d, e) while their compact-hexagonal-like organization is deduced from the surface plane views (panels b, g, h). These images exhibit PPNs with different pillar and roof height, structure, and composition, which are due to different adjustments of the chemical and processing conditions as it will be demonstrated further in the article.They have been obtained upon combining self-assembly of block copolymer,[6,7] nanostructured sol−gel coatings,[8] and highly controlled liquid deposition processing.[9] The structure contains two types of porosity. The first is the fully open and accessible interpillar porosity with characteristic dimensions adjustable between 20 and 200 nm, which is necessary to allow facile diffusion despite the double layer effect. The second is present inside the pillars and the roof, and is composed of less than 10 nm pores, which aim to increase the surface area. So far, and in the context of the present article, only the diffusion of water by capillarity has been tested to confirm that fluids can naturally enter dense and mesoporous PPN systems. The presence of mesoporosity is not expected to have a significant effect on this phenomenon since the filling will be mainly governed by the larger interpillar pores, as explained by the presently verified Washburn theory. On the other hand, micro- and nanofluidic devices are mainly designed to perform specific functions on solutes that diffuse by electro or osmophoresis within the fluid, or are conveyed by it by flow control, inside the channels. It is thus a prerequisite to be able to fill this PPN by fluids and to understand how natural capillary force governs the filling. The goal of creating mesoporosity in the PPN is mainly the significant increase of the surface area. The mesoporosity will thus have an effect when the PPN layers will be used to convey dissolved species, such as ions, proteins, DNA, and so forth, with the aim to concentrate, isolate, separate, react, condition, or analyze them. In analogy to hierarchical macro-mesoporous materials, used in catalysis and chromatographic

(6) Kim, H.-C.; Park, S.-M.; Hinsberg, W. D. *Chem. Rev.* **2010**, *110*, 146–177.
(7) Olson, D. A.; Chen, L.; Hillmayer, M. A. *Chem. Mater.* **2008**, *20*, 869–890.
(8) Sanchez, C.; Boissière, C.; Grosso, D.; Laberty, C.; Nicole, L. *Chem. Mater., special issue* **2008**, *20*, 682–737.
(9) Faustini, M.; Louis, B.; Grosso, D. J. Phys. Chem. **2010**, ID: jp-2009-114755.R1

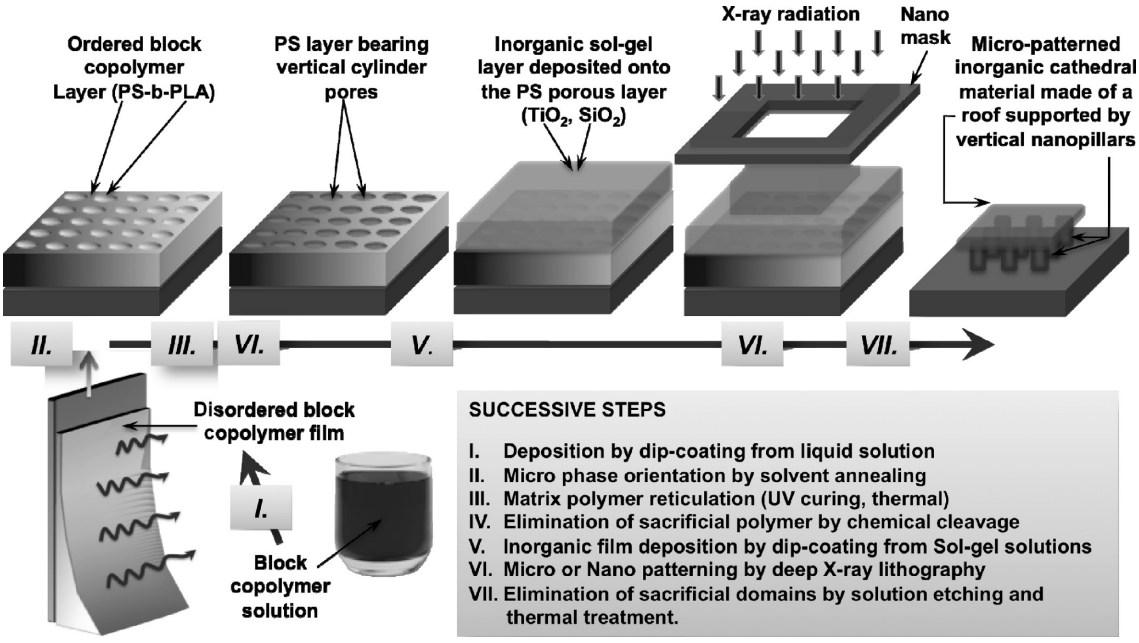

Figure 2. Scheme illustrating the various steps that can be successively applied to prepare the PPN layers. When step VI is not applied, the final system is a 2D-continuous layer with homogeneous structure. The lithography step VI can be applied either on the hybrid layer, after step V as shown in the present Figure, or right after step II on the pure polymer layer.

separation technologies,[10−12] the mesoporous PPN layers are expected to be much more efficient than dense PPNs. The continuous top roof layer protects the pillars against mechanical constraints and isolates the underneath porous network. We will also show that the preparation method allows for easy integration into fluidic devices, which is usually a limiting factor in nanofluidics. Indeed, the PPN preparation is fully compatible with top-down techniques, or with lithography such as deep X-ray lithography,[13,14] while it is fully compatible with PDMS related nano-in-micro technologies. All these characteristics make this system ideal media for nanofluidic applications[15,16] and more specifically for DNA stretching,[17−19] for separation,[20] for molecular concentrators,[21] and for chemical analysis.[22]

2. Experimental Section

PS porous layer preparation (steps I−IV in Figure 2): A solution of 20 mg of PS-b-PLA, namely, Polystyrene-b-Polylactide (obtained following the procedure described by Zalusky et al.[23] and having a total molecular weight of 90 000 $g \cdot mol^{-1}$, a PLA volume fraction of 34%, and a polydispersity index of 1.07) in 1 mL of chlorobenzene was transposed into the dip coater reservoir. Si wafer, or glass slide, substrates were then immersed into the solution and withdrawn at a constant speed. The atmosphere in the dip coater chamber was adjusted at 80 °C so as to speed up the chlorobenzene evaporation and improve the film thickness homogeneity. Thicknesses between 50 and 400 nm were obtained for withdrawal speeds ranging from 5 to 40 mm s^{-1}, respectively. Films were then exposed to the saturated tetrahydrofuran (THF) vapors for 4 h. For that purpose, samples were placed in a closed glass vessel (1.5 L desiccator) at 25 °C with a reservoir of solvent (15 mL) to reach in the vessel the saturated vapour pressure of the solvent Films were promptly removed from the vessel and allowed to dry at room temperature for a few minutes. Samples were exposed to UV light (wavelength 365 nm, power 40 W, distance = 20 cm, under air at 25 °C) for 1 h. The PLA sacrificial polymer is then selectively eliminated by hydrolysis of the PLA segments for 10 min in basic solution (MeOH, H_2O, NaOH 0.5 M).

Inorganic PPN Preparation (Steps V and VII in Figure 2). Absolute ethanol was purchased from Normapur and inorganic precursors ($TiCl_4$, TEOS (TetraEthylOrthoSilicate), Pluronic F127 (EO_{106}-PO_{70}-EO_{106}) and CTAB (CethylTriethylAmmonium Bromide) were purchased from Aldrich. Sol−gel films were deposited by dip-coating (step V) from fresh solutions having the following final molar compositions: 0.9 $TiCl_4$, 0.1 TEOS, 5 H_2O, 0.005 F127, and 40 EtOH for F127-templated titanosilicate films; 1 TEOS, 5 H_2O, 0.14 CTAB and 20 EtOH for CTAB-templated pure silica films; and 1 $TiCl_4$, 5 H_2O, and 40 EtOH for dense titania layers. Dip-coating in the sol−gel solutions were

(10) Minakuchi, H.; Nakanishi, K.; Soga, N.; Ishizuka, N.; Tanaka, N. *Anal. Chem.* **1996**, *68*, 3498–3501.
(11) Nakanishi, K.; Amatani, T.; Yano, S.; Yano, S.; Kodaira, T. *Chem. Mater.* **2008**, *20*, 1108–1115.
(12) Konishi, J.; Fujita, K.; Nakanishi, K.; Hirao, K.; Morisato, K.; Miyazaki, S.; Ohira, M. *J. Chromatogr., A* **2009**, *1216*, 7375–7383.
(13) Saile, V. *Introduction to LIGA and its applications in advanced micro and nanosystems*; Saile, V., Wallrebe, U., Tabata, O., Korvinke, G., Eds.; Wiley-VCH: Weinheim, *7*, 2009.
(14) Perennes, F.; De Bona, F.; Pantenburg, F. J. *Nucl. Instrum. Methods Phys. Res., Sect. A* **2001**, *1274*, 467–468.
(15) Eijkel, J. C. T.; Van Den Berg, A. *Microfluid. Nanofluid.* **2005**, *1*, 249–267.
(16) Abgrall, P.; NguyenN., T. *Anal. Chem.* **2008**, *80*, 2326–2341.
(17) Kaji, N.; Okamoto, Y.; Tokeshi, M.; Baba, N. *Chem. Soc. Rev.* **2010**, *39*, 948–956.
(18) Li, W.; Tegenfeldt, J. O.; Chen, L.; Austin, R. H.; Chou, S. Y.; Kohl, P. A.; Krotine, J.; Sturm, J. C. *Nanotechnology* **2003**, *14*, 578–583.
(19) Pearson, F.; Tegenfeldt, J. O. *Chem. Soc. Rev.* **2010**, *39*, 985–999.
(20) Daiguji, H. *Chem. Soc. Rev.* **2010**, *39*, 901–911.
(21) Kim, S. J.; Song, Y. A. K.; Han, J. *Chem. Soc. Rev.* **2010**, *39*, 912–921.
(22) Piruska, A.; Gong, M.; Sweedlerb, J. V.; Bohn, P. W. *Chem. Soc. Rev.* **2010**, *39*, 1060–1072.
(23) Zalusky, A. S.; Olayo-Valles, R.; Taylor, C. J.; Hillmyer, M. A. *J. Am. Chem. Soc.* **2001**, *123*, 1519–1520.

performed at room temperature, at ambient humidity and at withdrawal speeds ranging from 0.5 to 5 mm s^{-1}. In step VII, hybrid layers were directly calcined at 450 °C for 10 min (F127-templated titanosilicate films were aged for 12 h at 75% RH before thermal treatment).

Deep X-ray Lithography (Step VI in Figure 2). The as-deposited films were immediately patterned at the Deep X-ray Lithography beamline (DXRL) at Elettra synchrotron facility (Trieste, Italy). Samples were exposed through X-ray masks containing test patterns of different size, shape, and geometry (5 to 500 mm). The masks had a gold absorber 20 mm thick and a transparent titanium membrane with thickness of 2.2 mm. X-ray doses in the 6 to 12 kJ cm^{-3} range were used for patterning. After exposure to X-rays, the films were developed by chemical etching to remove the non-irradiated parts of the mesostructure. The etching solution was prepared by a mixture of ethylene glycol, acetone, and water. The films, after the lithographic process, were thermally treated at 450 °C for 10 min (step VII). Etching procedures are very difficult to optimize but are important steps that are not yet fully understood, even if dissolution and delamination are likely responsible for the selective elimination.

Structural Characterizations. Images of the PPN micro patterns after Deep-X-ray irradiation was observed with an optical microscope (Nikon Optiphot 500), both before and after the development. PPN structure were investigated using Field Emission Gun Scanning Electron Microscopy (SEM-FEG) Zeiss Ultra 55 at 0 and 90° incidence to see the profile. Grazing Incidence Small-Angle X-ray Scattering were first performed using GISAXS-Rigaku S-max 3000 equipped with a microfocus source $\lambda = 0.154$ nm and a two-dimensional (2D) Gabriel type detector place at 1480 mm from the sample as a routine analyzing platform. High quality patterns were obtained at the Austrian SAXS beamline of Elettra (Trieste-Italy). The incident X-ray beam (8 KeV) was collimated into a vertically elongated rectangular shape of 400 × 1000 μm. Small angle X-ray diffractions were collected in grazing incidence ($\omega \approx 0.25°$) on a CCD camera (Photonic) placed at a distance of 190 cm from the sample. The transmitted and specular reflected beams were masked by a vertical beam-stop. Diffraction patterns were analyzed using Igor software. Ellipsometry measurements were performed on a UV−visible (from 240 to 1000 nm) variable angle spectroscopic ellipsometer (VASE − 2000U Woollam), and the data analyses were performed with the Wvase32 software using Cauchy models for both layers. Environmental Ellipsometry Porosimetry was investigated through capillary condensation of water into the porosity using an atmospheric control chamber designed by SOPRA-LAB. Capillary filling investigation: water front propagation was recorded through the PDMS stamp using a Nikon Optiphot 500 optical microscope.

3. Results and Discussion

Strategy to Build up the PPNs. An illustration of the typical steps involved in the preparation of the PPN is shown in Figure 2. Deposition of the block copolymer PS-b-PLA was performed by dip-coating silicon or glass substrates into a 20 mg/mL PS-*b*-PLA solution (step I). The atmosphere in the dip coater chamber was adjusted to 80 °C so as to speed up the solvent evaporation and improve the film thickness homogeneity. Thicknesses were accurately adjusted between 50 and 400 nm by modulating the withdrawal speeds.[9] PS-b-PLA was chosen because of the high polarity contrast between both blocks, and because PLA could be easily and selectively eliminated by hydrolysis in basic media. However, commercial block copolymers containing PMMA, PVP, or PEO could also be used for such purposes. After deposition, the polymer film adopts a metastable structure for which randomly oriented nanodomains of PLA are surrounded by the PS phase. Polymer ordering (step II) was achieved by solvent annealing that drives the PLA domains to orient vertically with respect to the surface of the substrate.[24] The solvent imparts mobility to the copolymer, allowing morphological reorganization. The adopted structure depends on the selectivity of the solvent, the interfacial interactions and commensurability of the film. In this case, exposure to a saturated atmosphere of neutral solvent such as THF for moderate times (typically 4 h) leads to a hexagonal arrangement of perpendicularly oriented PLA cylinders. The latter perpendicular orientation was then stabilized by UV-curing (step III) during which PS chains are presumably cross-linked. The PLA sacrificial polymer was then selectively eliminated by hydrolysis (step IV) in basic media ($MeOH/H_2O$, NaOH 0.5 M). The polymer layer contains now nanopores running perpendicularly from the substrate to the surface, where the PLA domains previously stood. The simultaneous impregnation of the porosity and deposition of the top layer roof with inorganic precursors (step V) was performed by dip-coating because it is highly compatible with sol−gel chemistry through which the nature, structure, and porosity of the inorganic matrix can be selected from among the myriad of possible combinations.[8]

Inorganic F127-templated titanosilicate, and CTAB-templated pure silica sol−gel films were deposited by dip-coating (step V) from fresh solutions that contained $TiCl_4$ and/or TEOS as inorganic precursors and F127 and CTAB as mesostructuring agents respectively. Here again, this process allows for a perfect control of the quantity of deposited material, and therefore a fine adjustment of the roof thicknesss.[9]

At this stage, the system is composed of a partly condensed inorganic top layer, that fully penetrates the porosity of the underneath PS layer. It can then be permanently stabilized at 450 °C (step VII), which results in the simultaneous inorganic network polycondensation and the decomposition of the PS matrix. The F127 or CTAB mesostructuring agents, potentially present in the inorganic matrix are also decomposed at this temperature. When the stabilization (step VII) is directly applied after deposition of the inorganic material (step V), one ends up with a continuous and homogeneous layer of PPN extending over the entire substrate surface. Nevertheless, microstructuring of the PPNs layer into fluidic circuits can be obtained at different steps along the processing line by applying conventional, or less conventional, "top-down" methods such as Deep X-ray Lithography ((DXRL) Elettra synchrotron facility - Trieste, Italy) (step VI).[10,11] As illustrated in Figure 2, the PPN zones that are not covered by the mask are exposed to X-ray irradiation, locally causing

(24) Vayer, M.; Hillmyer, M. A.; Dirany, M.; Thevenin, G.; Erre, R.; Sinturel, Ch. *Thin Solid Films* **2009**, *518*, 3710–3715.

PS cross-linking,[25] PLA decomposition,[26] and inorganic network stiffening.[27,28] The pattern is then developed through careful chemical etching of the non-irradiated zones (mixture of ethylene glycol, acetone, and water). The films were then thermally treated at 450 °C for 10 min (step VII). Etching procedures are very difficult to optimize but are important steps that are not yet fully understood, even if dissolution and delamination are likely responsible for the selective elimination. Another possibility is to apply the lithography (step VI) directly on the polymer layer straight after the polymer ordering (step II). Both routes have been applied as illustrated by the optical images in Figure 1, panels h and i, where 40 μm hexagonal motifs have clearly been patterned.

Description of the Mesoporous PPNs Structure. PPN structures have been characterized by Grazing Incidence Small Angle X-ray Scattering (GI-SAXS) and by optical and electronic microscopies, while thicknesses and porosity were confirmed by spectroscopic ellipsometry. Microscopy images displayed in Figure 1 are representative of the whole system, and show the typical PPN layers made of dense and mesoporous materials organized into vertical nanopillars supporting a continuous roof. Pillars have dimensions that are directly dependent on pore dimensions in the PS membrane and thus are homogeneous in diameter and spacing. Thicker porous PS membranes lead to taller pillars. Concerning the roof, its thickness is directly related to the additional quantity of sol−gel materials that are deposited on of the PS layer after total filling of the PS vertical porosity. Here again, this thickness can be accurately controlled through careful adjustment of the conditions (e.g., dilution and withdrawal velocity). Global thicknesses between 50 and 140 nm are shown in Figure 1, while 500 nm thick films have been obtained to date (data not shown). However, care must be taken not to grow too thick a roof on top of the pillars as crack formation can occur upon thermal treatment (step VII). Pillar ordering can be assessed by GI-SAXS analysis as shown in Figure 3a for F127-templated titanosilicate systems and in Figure 4a for CTAB-templated silicate systems. In both cases, the intense Bragg diffraction signal at $q_y = 0.14$ nm^{-1}, together with its first harmonic at $q_y = 0.28$ nm^{-1}, is associated to both $(01)_p$ and $(02)_p$ diffractions of the highly ordered 2D lateral hexagonal structure formed by the pillar array with a corresponding interpillar distance of 51 nm ($d_{(01)} = 44$ nm) (see Figure 3b). The latter dimensions can be found on Transmission Electron Microscopy (TEM) and Scanning Electron Microscopy (SEM) images whatever the type of inorganic material used for impregnation. The fact that the $(01)_p$ diffraction has a vertical tail (diffraction rod) extending

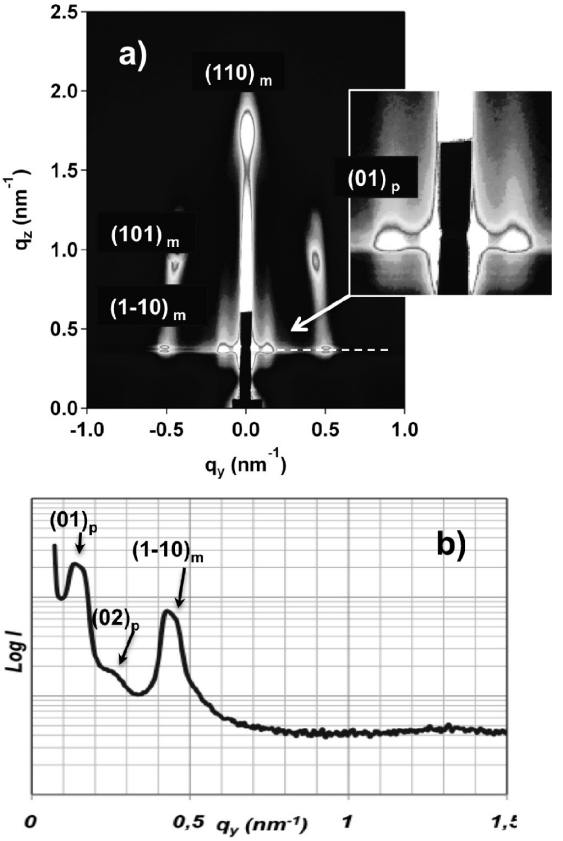

Figure 3. (a) GI-SAXS pattern of typical (F127-templated) 10%SiO_2-90%TiO_2 PPN, exhibiting the typical Bragg points of a *Im3m* mesostructure at higher q-value and the diffraction rods associated to the pillar periodicity at lower q-values. (b) Plot of the diffused intensity (log I) versus the wave vector in the y direction of the reciprocal space, showing both lateral periodicities.

only in the z direction, suggests a high degree of vertical alignment of the pillars. For the F127-templated titanosilicate layers, the GI-SAXS diagram Figure 3a exhibits, together with the previous $(01)_p$ diffractions of the pillars at low q, the characteristic $(110)_m$, $(101)_m$, and $(1-10)_m$ diffraction points of the *Im3m* mesostructure, revealing that the nanoporous network is composed of contracted body center cubic arrangement of pores with extended domains having the [110] direction normal to the surface.

The lateral periodicity is found to be 14.5 nm, which corresponds to the structure obtained for plain continuous films, for which pores sizes were deduced from ellipsometry porosimetry to be around 6 nm.[29] The highly ordered structure is clearly observed in SEM and TEM images in Figures 1c−f. Interestingly, the SEM image (c) reveals that the pillars do not have the same texture as the roof. TEM image of Figure 1f shows that the pillars are actually hollow cylinder (tubes) below the roof. It is possible that the confinement drives the F127 to form cylindrical micelles that have then no other choice than to adapt the less energetically favorable configuration, that is, to align themselves in the pillars longer direction. In addition, in this configuration, the inorganic hydrophilic species are favorably interacting with the −OH groups left on the PS

(25) Kizilkaya, O.; Ono, M.; Morikawa, E. *J. Electron Spectrosc. Relat. Phenom.* **2006**, *151*, 34–39.
(26) Wollersheim, O.; et al. *Nucl. Instrum. Methods Phys. Res., Sect. B* **1995**, *97*, 273–278.
(27) Falcaro, P.; Costacurta, S.; Malfatti, L.; Takahashi, M.; Kidchob, T.; Casula, M. F.; Piccinini, M.; Marcelli, A.; Marmiroli, B.; Amenitsch, H.; Schiavuta, P.; Innocenzi, P. *Adv. Mater.* **2008**, *20*, 1864–1870.
(28) Falcaro, P.; Malfatti, L.; Vaccari, L.; Amenitsch, H.; Marmiroli, B.; Grenci, G.; Innocenzi, P. *Adv. Mater.* **2009**, *21*, 4932–4936.
(29) Sakatani, Y.; Grosso, D.; Nicole, L.; Boissiere, C.; Soler-Illia, G.J. de A.A.; Sanchez, C. *Chem. Mater.* **2006**, *16*, 77–82.

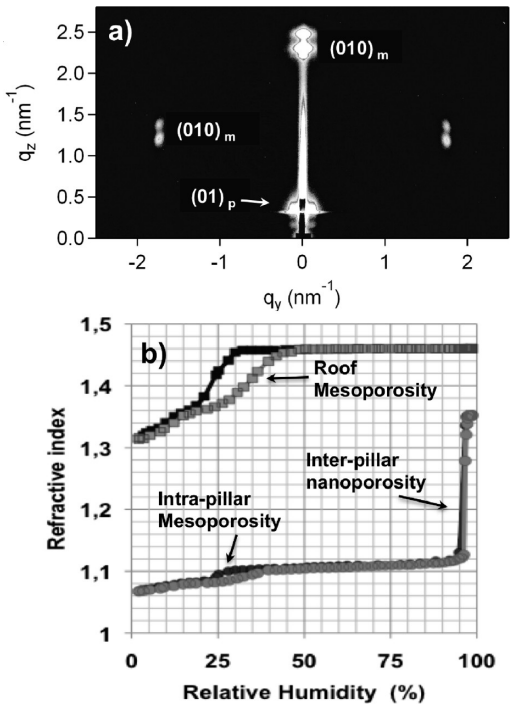

Figure 4. (a) GI-SAXS pattern of a *p6m* mesoporous (CTAB templated) 100%SiO_2 PPN, exhibiting the typical Bragg points of a *p6m* mesostructure at higher *q*-value and the diffraction rods associated to the pillar periodicity at lower *q*-values. (b) Adsorption/desorption isotherms of the *p6m* mesoporous roof top-layer and of the pillared underneath layer, corresponding to the variation of refractive index upon water vapor exposure.

walls after cleavage of PLA, The High-Resolution Transmission Electron Microscopy (HR-TEM) image in Figure 1g shows a transversal cut of one pillar, clearly depicting the empty center and the surrounding continuous wall. The same confinement effect on the self-assembly of inorganic precursors in presence of F127 inside tube-like pores of anodized alumina membranes has previously been observed by Stucky's group.[30] It is thus very probable that the tube-like geometry of the confining cavities induces the F127 micelle orientation parallel to the walls. This latter hollow structure causes weak diffused scattering in the present GI-SAXS geometry. The GI-SAXS pattern of CTAB-templated silica system displayed in Figure 4a also reveals the presence of the pillar organization together with a mesostructure. Indexing the diffraction points allows to state that the porous network is composed of cylindrical pores organized into a 2D-hexagonal (space group *p6m*) structure with the c6 axes laying horizontally. As expected the periodic distance is found at much higher *q* values ($d_{(10)}$ = 2.95 nm) than for the F127-templated system. Once more this is a typically previously reported structure for such a CTAB templated silica materials.[31] Porosities of the latter system were investigated by Ellipsometry Porosimetry. Two independent transparent layers, pillared and roof, were use to model the PPN layer. The diagram in Figure 4b represents the adsorption/desorption isotherms of water inside the pillared underneath layer (orange and red curves) and the top-roof layer (light and dark blue curves). The top layer presents the typical adsorption/desorption curves of CTAB-templated films with capillary condensation taking place at 35% RH, which corresponds to pores of diameter below 2 nm.[32] Water desorption takes place at a lower pressure of 25%, suggesting the presence of narrower restrictions between pores.

The underneath layer exhibits the same adsorption desorption hysteresis but with a much lower variation of refractive index, confirming the presence of the same type of porosity inside the pillars. In addition, a significant refractive index increase occurs at higher humidity (95% RH), which is attributed to interpillar porosity with no evident restriction revealed by the lack of hysteresis. At such pressures, pore diameters can be estimated to be over 20 nm in dimension with a fully open geometry.[33] This investigation confirms that mesoporosity is present in both the pillars and the roof materials with the same type of pore distribution, while a much greater porosity is due to the interpillar void within the underneath layer. Using the Bruggeman Effective Medium Approximation, the roof porosity was estimated to be 35% vol., while 70% vol. of the underneath layer is composed of the interpillar void (20% vol is composed of SiO_2).

Application as PPNs. Controlling the diffusion of fluids and solutes inside submicrosize channels is a key point for lab-on-chip devices. Indeed, when the wall-to-wall distance is below twice the value of the Debye length (i.e., usually below 50 nm), electrostatic interaction governs the diffusion. On the other hand, steric interactions play a key role when channels become smaller than 5 nm. The latter interactions more and more strongly affect the fluid and solute physical-chemical properties with decreasing channel dimensions.[34] The difficulty remains in taking maximal advantage of such wall-proximity properties together with promoting diffusion at millimeter length-scales. The PPNs gather both characteristics as shown by the capillary filling experiments described in Figure 5. Here, water was allowed to diffuse into a nanofluidic diffusion path that was created by simply applying a PDMS stamp (hand-cut with a surgical blade) on top of a PPN layer deposited onto a silicon wafer. The PDMS stamp has several roles that are as follows: (i) isolating the reservoir entrance zone (A) for the water drop to be deposited, (ii) allowing the water flow to be laterally confined only underneath the PDMS, and (iii) preventing water to pervaporate through the porous roof layer.[35] The distance between entrance and exit (A to B) edges was 1.5 mm. The width of the path was 4 mm in the experiment and corresponds to the width of the PDMS stamp.

(30) Wu, Y. Y.; Cheng, G. S.; Katsov, K.; Sides, S. W.; Wang, J. F.; Tang, J.; Fredrickson, G. H.; Moskovits, M.; Stucky, G. D. *Nat. Mater.* **2004**, *3*, 816–822.
(31) Grosso, D.; Boissière, C.; Nicole, L.; Sanchez, C. *J. Sol-Gel Sci. Technol.* **2006**, *40*, 141–154.
(32) Bass, J. D.; Grosso, D.; Boissiere, C.; Coradin, T.; Sanchez, C. *Chem. Mater.* **2207**, *19*, 4349–4356.
(33) Boissiere, C.; Grosso, D.; Sophie, L.; Nicole, L.; Brunet-Bruneau, A.; Sanchez, C. *Langmuir* **2005**, *21*, 12362–12371.
(34) Eijkel, J. C. T.; van den Berg, A. *Chem. Soc. Rev.* **2010**, *39*, 957–973.
(35) Grosso, D., Linden, M.; Sanchez, C. Dispositif micro-fluidique pour convoyer un produit par diffusion dans substrat poreux. French Patent 9F-143-Cas 12 BP. FR_09_02753.

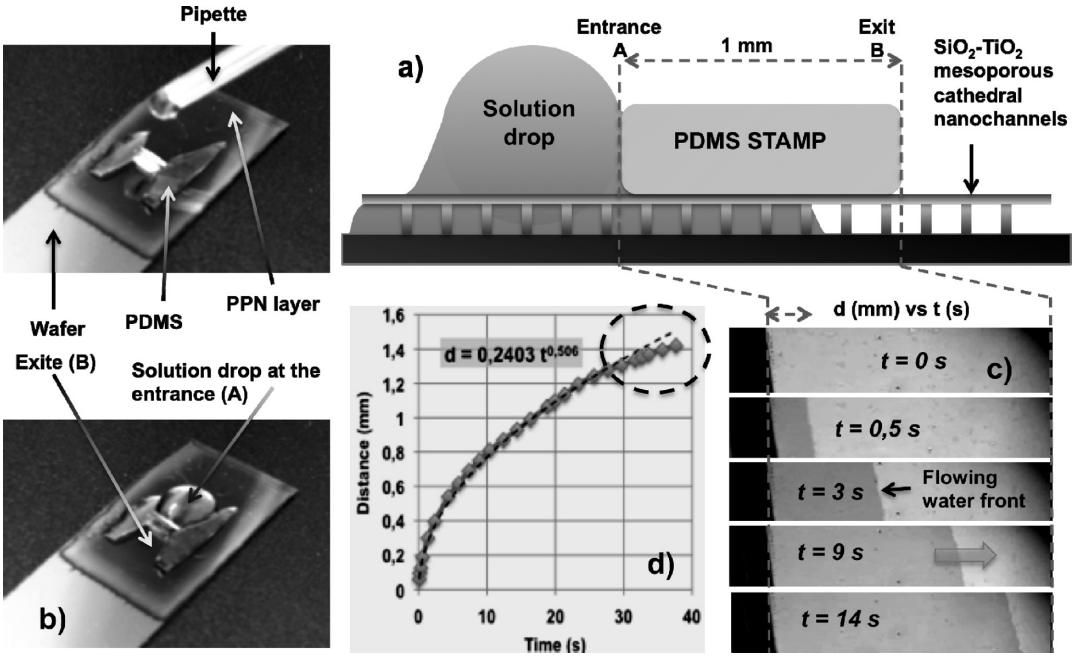

Figure 5. (a) Scheme of the device used to investigate the water capillary filling inside the PPN. (b) Image of the PDMS stamp simply applied on the surface of the PPN layer. The propagation front of the water inside the PPN layer, beneath the PDMS, with time is shown in (c). (d) Diagram of the water front displacement versus time.

When a water drop is deposited at the entrance edge A, a wetting front rapidly develops underneath the PDMS and propagates in the direction that is normal to the PDMS edge. The latter water flow is shown in the optical microscope images of Figure 5c at different times. Water filling induces an optical density increase of the PPN. The longitudinal homogeneity of the water front suggests that the dynamic of filling is equal all along the entrance edge A and remains so all across the layer, which is associated to the high homogeneity of the PPN structure. Plot of distance (d) versus time (t) in Figure 5d displays the characteristic parabolic trend of a diffusion-limited phenomenon.

These data can thus be fitted with a mathematical equation in which d is linear with time t to the power of 1/2. This is verified up to the last 0.5 mm from the exit edge B where the filling is much lower than what is expected from the fit. The latter deviation is likely due to the water pervaporation driven at the exit edge B, slowing down the water filling. This phenomenon is responsible for the confinement of the fluid underneath the PDMS, since no water filling is observed to pass this limit. Obviously, this pervaporation is governed, and can thus be controlled, by the atmospheric relative vapor pressure which was 40% RH for the present experiment.

Fluid capillary filling is induced by the negative Laplace pressure and has been first modeled by Washburn[36] for circular channels, and adapted to *plain* planar nanochannels by Han et al.[37] This theory suggests that the filling speed u is determined by $u = D^{1/2}.t^{1/2}$, where the diffusion constant $D = (h\gamma \cos\theta)/(3\eta)$ (h, γ, θ, and η are the planar nanochannel height, the fluid surface tension, dynamic contact angle, and viscosity, respectively). This theory is partly verified for our system since it really follows a diffusion-limited behavior, but D is 4 to 6 times lower than what has been recently reported for pillar-free planar nanochannels and water fluid.[33,38,39] Such a difference is certainly related to the presence of nanopillars that significantly increase the quantity of interface. The fraction of water molecules submitted to the hydration force at the solid interface is higher, which results in an increase of the apparent viscosity.[33−35] In this configuration, evaporation, taking place at the edge of the impermeable PDMS, is confining water into the planar nanochannel. The roof is sealing the interpillar porosity and additionally provides the mechanical stability to the underneath pillar-layer. It also prevents the water to be in direct contact with the PDMS. The same experiment performed with a plain mesoporous layer, no PPN structure, does not show efficient diffusion certainly because of the small pores and tortuousity.

4. Conclusion

In summary, the described Mesoporous Pillared Nanochannel layers are easy to produce on large surfaces through a bottom-up process that does not involve expensive equipment. They have the ability to convey fluids, and certainly solutes, exactly as microfabricated ones do, with the advantages of being able to tune the materials porosity, composition, and surface through a combination with sol−gel chemistry. They are compatible with lithography

(36) Washburn, E. W. *Phys. Rev.* **1921**, *17*, 273–283.
(37) Han, A.; Mondin, G.; Hegelbach, N. G.; de Rooij, N. F.; Staufer, U. *J. Colloid Interface Sci.* **2006**, *293*, 151–157.
(38) Haneveld, J.; Tas, N. R.; Brunets, N.; Jansen, H. V.; Elwenspoek, M. *J. Appl. Phys.* **2008**, *104*, 014309.
(39) Van Honschoten, J. W.; Brunets, N.; Tas, N. R. *Chem. Soc. Rev.* **2010**, *39*, 1096–1114.

techniques for complex micro/nanopattern designs and can find direct lab-on-chip applications by simply applying a PDMS stamp to the surface to laterally confine the fluids underneath the stamp. At a time when constructing a nanofluidic device is far from accessible to all scientists, we believe that the present low-cost PPN layers will have a promising future in the domain of lab-on-chip, as well as in other domains such as optics, sensing, and electronics for which additional investigations are in progress.

Acknowledgment. Dominique Jalabert and Stephan Borensztajn are thanked for TEM and SEM analyses. The authors also acknowledge funding provided by the CNRS and the UPMC.